RSC Advances

PAPER

View Article Online
View Journal | View Issue

Cite this: *RSC Adv.*, 2024, **14**, 15048

Improving photoluminescence properties and reducing recombination of $CsPbBr_3$ perovskite through lithium doping

Hicham Zalrhi, [a] Mouad Ouafi,[be] Mohammed Regragui,[a] Bernabé Marí Soucase,[d] Faisal Baig,[c] Yousaf Hameed Khattak, [c] Ullah Shafi, [d] Mohammed Abd-lefdil[a] and Lahoucine Atourki *[a]

This study investigates the impact of lithium doping on the structural and photophysical properties of spin-coated $CsPbBr_3$ perovskite thin films. The deposited films display a pristine structure, preferentially growing along the (220) direction, and exhibit high-quality green photoluminescence at around 530 nm. The doping leads to an improvement in the optical properties of the films, as evidenced by a stronger photoluminescence (PL) intensity compared to undoped $CsPbBr_3$, particularly at temperatures below 200 K. The increase in PL intensity suggests a decrease in defects and surface passivation. Additionally, the decrease in the power-law exponent β from 1.6 to 1.0 indicates a reduction in non-radiative recombination, likely due to trap states filling with free electrons induced by the doping. Overall, doping with lithium reduces non-radiative recombination, fills trap states, and reduces band tail/activation energy, leading to improved optoelectronic properties of the films. This investigation provides insights into the photophysical properties of the Li–$CsPbBr_3$ absorber layer and the recombination mechanism, and helps to unravel new methods for the development of high-stability, high-performance perovskite thin-film solar cells and optoelectronic devices.

Received 29th February 2024
Accepted 23rd April 2024

DOI: 10.1039/d4ra01548g

rsc.li/rsc-advances

Introduction

Cesium lead halide perovskites show better moisture, oxygen, and thermal stabilities,[1–3] along with improved mechanical properties when organic cation (MA^+/FA^+) is substituted in perovskite solar cells,[4] allowing them to withstand temperatures up to 300 °C.[5] $CsPbBr_3$ exhibits remarkably high carrier mobility, large diffusion length, low trap density, and excellent light absorption.[6–9] In addition, $CsPbBr_3$ materials are known to have excellent optoelectronics characteristics, such as high quantum yield, excellent photophysical properties and strong light absorption,[10] which allow them to be successfully applied in photodetectors,[11,12] colored-light-emitting diodes[13,14] solar cells[11,13] and luminescent solar concentrators.[14] Furthermore, due to the bonding–antibonding interaction between the conduction and valence bands, $CsPbBr_3$ is a defect-tolerant semiconductor material that can maintain its general qualities despite the presence of defects.[15] Nevertheless, its remarkable photophysical properties, including lifetime, diffusion length, and recombination of carriers, can be affected by the defect density, and hence limit the device performance due to non-radiative losses.[16–18] The typical trap state density in solution-processed perovskite films is about 10^{15}–10^{16} cm^{-3}, which is comparable to the density of photogenerated or photoinjected carriers in solar cells or LEDs under device working conditions.[19,20] J. Kang and his colleagues performed theoretical calculations on $CsPbBr_3$. They suggested that the dominant defects can introduce shallow transition levels, and proposed that Br-poor growth conditions are a key factor for reducing the defect density.[15] Doping with alkali cations is a good way to reduce defects and therefore lower non-radiative recombination in perovskite materials. Various reports demonstrated the effect of doping on surface passivation, enlarging grain sizes, and passivating grain boundaries, as well as in reducing non-radiative losses and defect state density.[21,22] In particular, doping with alkali metal (Cs^+, Rb^+, Li^+, K^+) has been used as an effective way to reduce non-radiative losses in perovskite materials, either by grain and surface passivation or by suppressing the trapping of photo-carriers.[23–25] Alkaline doping (Rb^+, K^+, Na^+, …) enhances perovskite film performance, with less trap states and grain boundary passivation increasing the built-in potential, which as result leads to superior power conversion efficiency.[21,26–28] In fact, it has been observed that the alkaline metals Na^+ and K^+ exhibit a positive influence on the characteristics of solar cells, particularly in enhancing the

[a]*MANAPSE Lab, Faculty of Science, Mohammed V University in Rabat, Morocco. E-mail: l.atourki@um5r.ac.ma*
[b]*LRST, ESEFA, Ibn Zohr University, Agadir, Morocco*
[c]*Federal Urdu University of Arts, Science and Technology, Islamabad, Pakistan*
[d]*IDF, Polytechnic University, Spain*
[e]*LMER, Faculty of Science, Ibn Zohr University, Agadir, Morocco*

power conversion efficiency (PCE). For instance, the PCE showed significant improvement, rising from 15.56% to 18.16% and 17.81% with 1% Na doping and K doping respectively. As reported by the authors Wangen *et al.*,[21] this observed enhancement can be attributed to certain positive morphological changes in the $CH_3NH_3PbI_3$ perovskite materials. Rubidium has proven to be an efficient alkali metal for various optoelectronic devices, such as LEDs, as reported by Shi *et al.*[29] Their research revealed that the incorporation of Rb^+ in $FAPbBr_3$ significantly enhances the photoluminescence quantum yield (PLQY) by reducing trap density. Consequently, this improvement augments the performance of PeLEDs (perovskite light emitting diodes). An optimum PCE of 25.6% (certified 25.2%) has been reached for formamidinium lead triiodide ($FAPbI_3$) films, which have 450 hours of stability.[30] However, organic–inorganic perovskites suffer from device degradation due to hydrate formation.[31] The bandgap of $CsPbX_3$ (X: I, Br, Cl) can be adjusted from the visible to the ultraviolet by using different halide ions.[32,33] Among them, $CsPbBr_3$ with a 2.3 eV bandgap demonstrates superior phase stability under ambient conditions[34] with PCE values ranging from 2% to 8.29%.[35–38] Several studies have concentrated on exploring the impact of lithium on perovskites. For instance, H. Wu *et al.*[39] utilized LiBr within colloidal $CsPbX_3$ (X = Br and I) perovskite quantum dots as a novel agent aimed at mitigating defects for excited electrons. This approach significantly reduced non-radiative recombination, leading to enhanced performance. Their findings suggest that an optimal concentration of LiBr not only diminishes defects, but also enhances phase stability by mitigating halide migration effects. Another study conducted by Dazhao *et al.*[40] showed the self-crystallization of $CsPbBr_3$ nanocrystals within borosilicate glass through lithium doping. They elucidated that the introduction of lithium into $CsPbBr_3$ nanocrystals facilitated self-crystallization, which was primarily attributed to alterations in the glass network structure and an enhancement in the degree of phase separation within the glass.

In the present study, the impact of different fractions of Li doping on the structural, morphological, optical and photoluminescence properties is investigated. The mechanism of lithium doping on photocarrier recombination and its impact on deep defect trap states in $CsPbBr_3$ films are examined with the temperature and power dependence in photoluminescence characterizations. These findings also clarify the nature of the surface trap states and the role of lithium in the surface passivation of perovskite films.

Experimental details

Synthesis and characterization

Preparation of the substrate. FTO substrates were cleaned under sonification for 15 min, with 2% Hellmanex solution, acetone, and ethanol, respectively. Perovskite solution preparation: $CsPbBr_3$ films were synthetized from the appropriate molar ratio of CsBr (purity = 99.999%), LiBr (purity > 99%), and $PbBr_2$ (purity ≥ 98%), which were purchased from Sigma-Aldrich. The precursors were dissolved in 48% DMSO and 52% DMF under an inert atmosphere in an Ar filled glove box (O_2 and H_2O < 2 ppm). The solution was rigorously stirred at 80 °C for 24 hours.

Perovskite film deposition. The films were elaborated within the glove box *via* a spin-coating process at 5000 rpm for 30 s. Subsequently, the samples were dried and annealed at 90 °C for 30 min. Finally, the synthetized thin films were stored in the glove box before any analysis.

Perovskite film characterizations. A RIGAKU Ultima IV X-ray diffractometer was employed for structural studies using the Bragg–Bentano configuration. The surface morphology of the synthetized perovskite films was recorded using an environmental scanning electron microscope FESEM (Quanta 200 FEI). The optical absorption was measured using an Ocean Optics HR4000 spectrophotometer equipped with a Si-CCD detector. Photoluminescence characterizations were carried out using a He–Cd laser source and a back-thinned Si-CCD detector.

Results and discussion

Fig. 1a presents the X-ray analysis of the pristine and doped $CsPbBr_3$ films. The obtained patterns reveal several diffraction peaks, centered at 15.21, 21.6 and 30.6°, assigned respectively to the (110), (020), and (220) lattice planes, as shown in Fig. 1a. The asterisk symbol indicates the substrate contribution, and no binary phases were found within the detection limit of the instrument. The (220) peak intensity is relatively high compared to the literature data,[39–41] indicating preferential growth along this direction for the perovskite films. Furthermore, an increase in the (110) and (220) peak intensities is observed with doping, resulting in improved crystallinity of the synthetized films. The crystal structure of the obtained XRD results can be assigned to the cubic structure related to the space group $Pm\bar{3}m$.[42] Pawley refinement (Fig. 1d) was used to extract the lattice parameters of the undoped and Li^+ doped $CsPbBr_3$, as presented in Table 1. After a thorough analysis of the XRD results, it was observed that the incorporation of 0 to 5% Li alkali into the perovskite matrix results in a slight shift towards lower angle, as illustrated in Fig. 1b. This shift will notably influence the d-spacing according to Bragg's law and consequently affect the lattice parameters of the cubic structure. Fig. 1c illustrates the evolution of the lattice volume with the incorporation of Li into the $CsPbBr_3$ lattice, showing a consistent linear increase in volume with increasing Li content. This crystal expansion supported by higher lattice parameters was also reported by Z. Tang *et al.*,[43] who attributed it to the smaller ionic radius of the Li^+ alkali ions.

The FESEM images of undoped and doped 5% Li–$CsPbBr_3$ films are illustrated in Fig. 2a and b. A rougher and more compact film with a smaller grain size are observed for the pristine film (0% Li^+). In addition, its surface is well covered with regular grains distributed uniformly. In contrast, the doped film presents a surface covered with large regular grains. In fact, the grains sizes range from 300 to 600 nm. However, it suffers from the presence of pinholes, which may be attributed to the evaporation of DMF/DMSO as discussed in our recent works.[44] Upon comparing the morphology of both films, it is

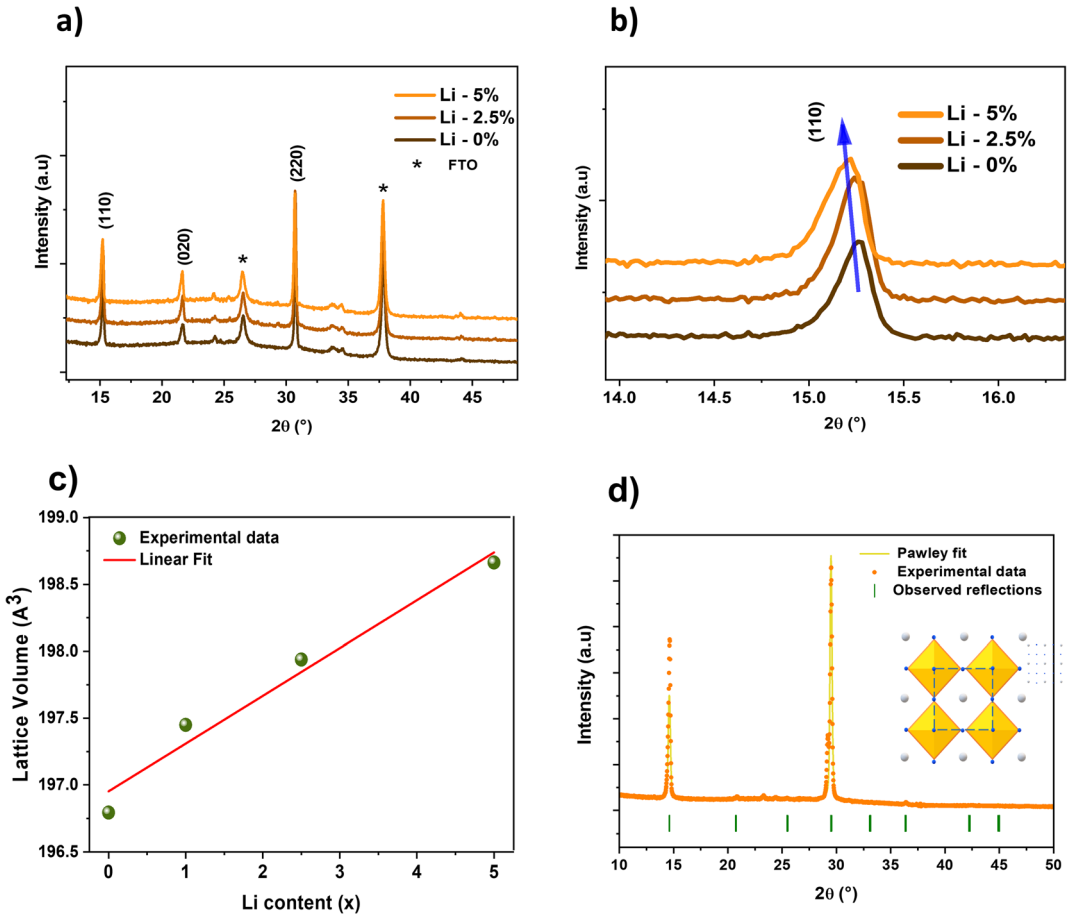

Fig. 1 (a) XRD pattern of spin coated $CsPbBr_3$ films with different Li contents (0, 2.5 and 5%). (b) Expansion of the XRD pattern within the angular range of 14–16.5°. (c) Lattice parameter evolution as a function of Li content. (d) X-ray diffraction pattern of $CsPbBr_3$: experimental and refinement data.

Table 1 Lattice parameters and R_P of undoped $CsPbBr_3$ and doped Li%–$CsPbBr_3$

Material	$CsPbBr_3$	2.5% Li–$CsPbBr_3$	5% Li–$CsPbBr_3$
Space group	$Pm\bar{3}m$	$Pm\bar{3}m$	$Pm\bar{3}m$
a (Å)	5.817 ± 0.001	5.828 ± 0.001	5.835 ± 0.001
R_p	7.78%	5.14%	4.15%

evident that the incorporation of Li^+ contributes to the enlargement of the grain size.

The room temperature optical absorption and photoluminescence emission relationships for the spin coated $CsPbBr_3$ film are illustrated in Fig. 2c. The sample exhibits a continuous increase in absorbance to reach an absorption edge at 2.37 eV and small excitonic features around 2.26 eV. The PL measurements reveal a sharp emission peak centered at 2.3 eV with a slight full width at half maximum (FWHM) of 20.66 nm. Stokes shifts are regularly observed in perovskite semiconductors and can be understood through a spectral diffusion/exciton relation process.[45] The inset shows the $CsPbBr_3$ crystal structure and the high green PL emission under an excitation of 405 nm.

The normalized photoluminescence spectra were evaluated at several temperatures from 30 K to 300 K for the $CsPbBr_3$ and 5% Li–$CsPbBr_3$ films, as illustrated in Fig. 3a and 2b, respectively. For both samples, the intensity of the PL peak decreases with increasing temperature, and the emission peak is blue-shifted and the FWHM values are enlarged due to the enhanced coupling with optical phonons[46,47] and can be attributed to the phonon-assisted broadening effect.[48] Furthermore, the PL intensity of the Li-doped $CsPbBr_3$ films was stronger than that of undoped $CsPbBr_3$ for operating temperatures below 200 K, which could be linked to an improvement in the optical properties of the films after doping. A slight shift is observed in the PL peak with temperature for the undoped and doped films, which suggests smaller differentiation in the bandgap.

To provide more information regarding the quality of the Li–$CsPbBr_3$ films, the exciton (electron)–phonon interaction processes, and the presence and nature of defects in their surfaces, temperature-dependent photoluminescence was carried out. Fig. 3a and b display the evolution of the integrated PL intensity for the undoped $CsPbBr_3$ and 5% Li–$CsPbBr_3$ films, respectively, at temperatures ranging from 30 to 300 K. The decrease observed in the integrated PL intensity with

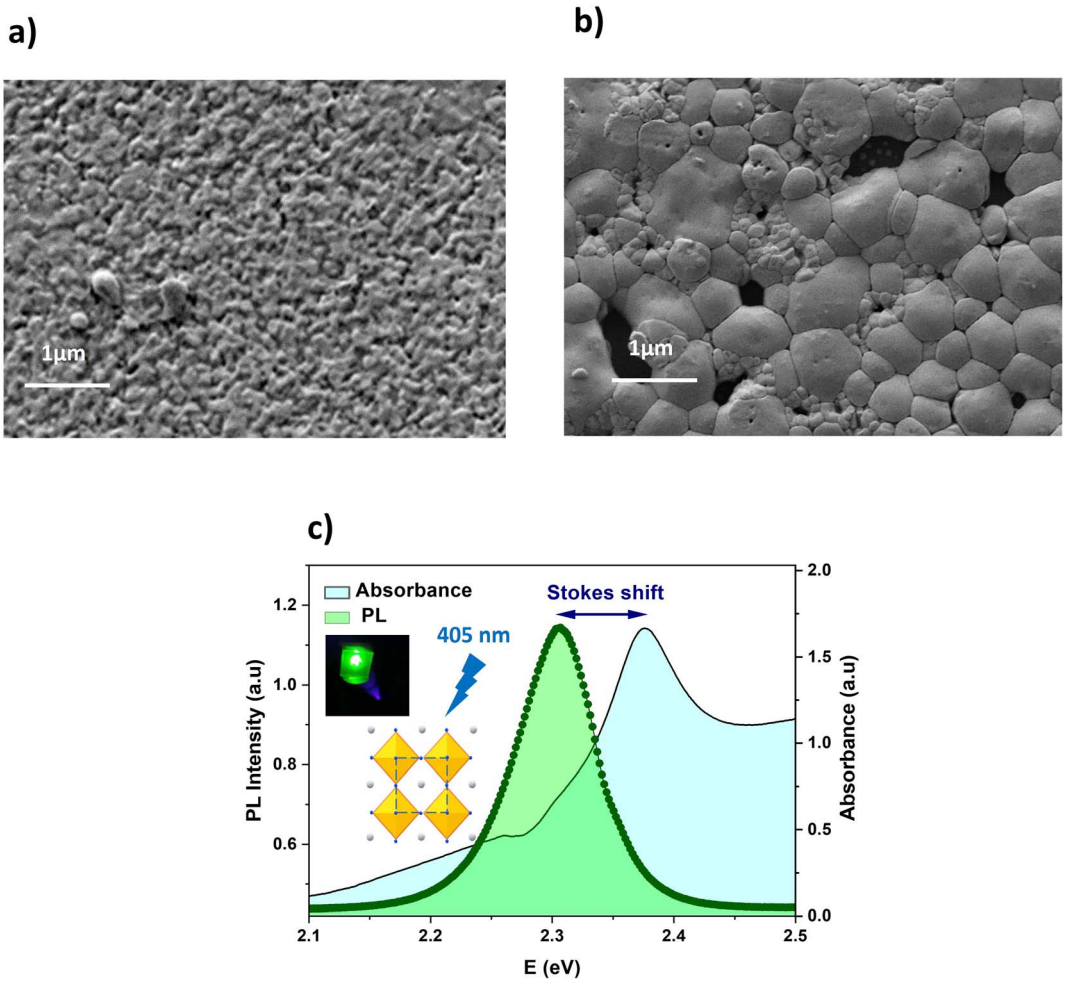

Fig. 2 (a) SEM image of undoped $CsPbBr_3$ film, (b) SEM image of 5% Li–$CsPbBr_3$ film, and (c) room temperature absorption and PL spectrum of $CsPbBr_3$ thin film.

temperature suggests the presence of thermal quenching.[49] Exciton dissociations are activated by thermal energy, which make them competitive with the radiative recombination.

A modified Arrhenius formula was used to fit the temperature-dependent integrated PL intensities, as presented in Fig. 4a. With increasing temperature, the integrated PL

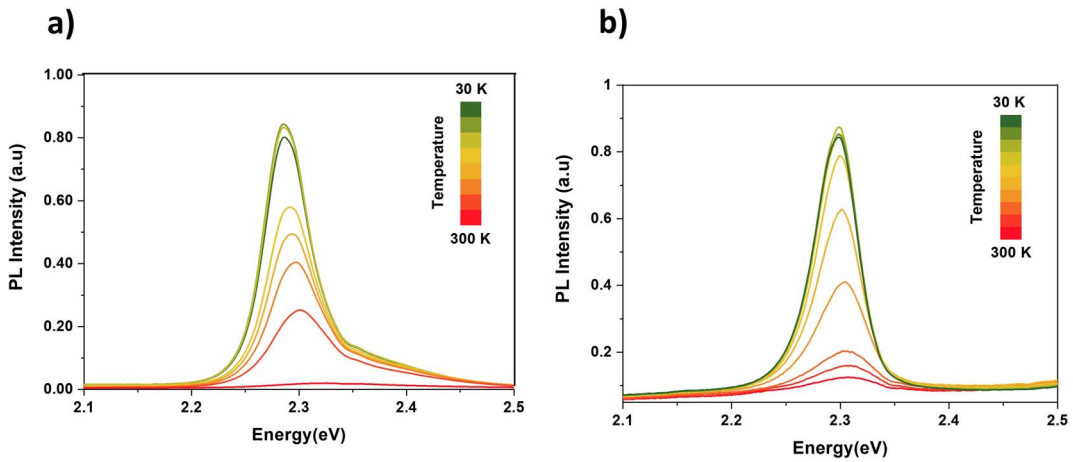

Fig. 3 Temperature dependent photoluminescence spectra in the temperature range of 30 K to 300 K for (a) $CsPbBr_3$ and (b) 5% Li–$CsPbBr_3$.

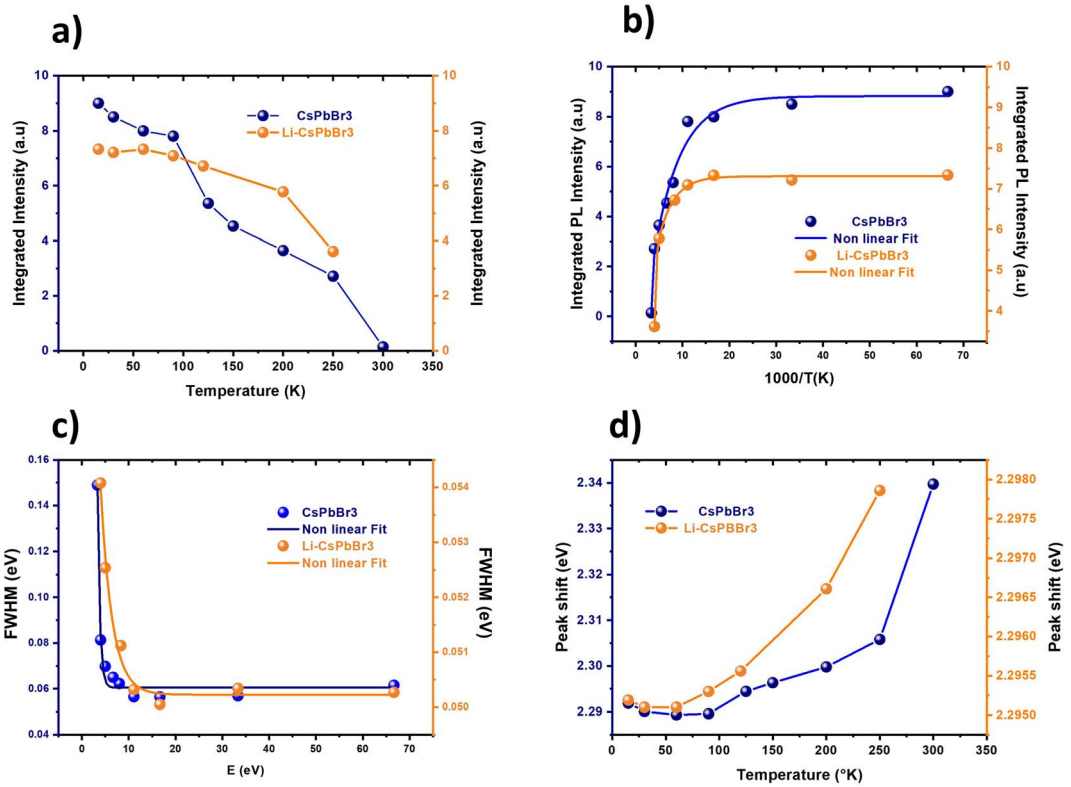

Fig. 4 (a and b) Evolution of integrated PL intensity with temperature for $CsPbBr_3$ and 5% Li–$CsPbBr_3$. (c) FWHM of the PL peak as a function of temperature for the $CsPbBr_3$ and 5% Li–$CsPbBr_3$ samples. (d) Peak shift of the $CsPbBr_3$ and 5% Li–$CsPbBr_3$ films with temperature.

intensity decreases, which suggests the appearance of thermal quenching.[49] The same exponential trend is observed in $CsPbBr_3$ nanocrystals and quantum dots.[46,50]

The activation energy was extracted from the Arrhenius equation:[51,52]

$$I(T) = \frac{I_0}{1 + a\exp\left(\frac{-E_a}{k_B T}\right)} \quad (1)$$

where I_0 represents the integrated PL intensity near 0 K, E_a is the activation energy of the non-radiative recombination process, a is related to the density of non-radiative recombination centers, and k_B is the Boltzmann constant.

The obtained exciton binding energy for $CsPbBr_3$ and 5% Li–$CsPbBr_3$ were found to be 60.50 and 50.22 meV, respectively. The obtained values are close to the ones reported in the literature.[46,53,54]

Emission linewidth can provide details about temperature-independent inhomogeneous broadening due to elemental composition, shape, or size dispersion. The contribution of exciton interactions with optical and acoustic phonons can also be provided by temperature-dependent homogenous broadening and are mainly due to lattice vibrations.[54] The mechanism of electron–phonon coupling is ascribed to the Boson model[55] and evaluated by fitting the FWHM of the PL emission with temperature as presented in Fig. 4c using the equation below:

$$\Gamma(T) = \Gamma_0 + \gamma_{ac}T + \frac{\gamma_{LO}}{\exp\left(\frac{E_{LO}}{k_B T}\right) - 1} \quad (2)$$

where Γ_0 refers to the inhomogeneous broadening, which involves the scattering process from disorder and lattice imperfections,[56] and γ_{ac} is the contribution of the exciton–acoustic phonon coupling coefficient. The third term represents the contribution of exciton interactions with longitudinal optical phonons, in which γ_{LO} is the coupling coefficient of the exciton–optical phonon, E_{LO} represents the phonon energy and k_B is the Boltzmann constant. The contribution of impurities was neglected in this calculation because of the minimal trap states in $CsPbBr_3$. It was found that the Gauss-fitted FWHM of the PL band increases with temperature.

Table 2 summarizes the fitting results for Γ_0, γ_{ac}, γ_{LO} and E_{LO}. The exciton–LO phonon coupling is the dominant contribution in homogenous linewidth broadening due to the polar nature of $CsPbBr_3$. Typically, the interactions between LO phonons and electrons are stronger than those between acoustic phonons and electrons.[57] The acoustic phonon

Table 2 Extracted PL linewidth broadening parameters

Sample	Γ (meV)	γ_{ac} (meV K^{-1})	γ_{LO} (meV)	E_{LO} (meV)
$CsPbBr_3$	61.55	1.40	84.8	33.43
5% Li–$CsPbBr_3$	50.22	0.24	51.96	1.23

interaction seems to have a negligible contribution to the FWHM of the PL emission.

The PL peak shifted to higher values with temperature for both the spin-coated films, as shown in Fig. 4d, which could be due to lattice dilatation and crystallite reorientation.[9] The peak position increases moderately for the doped film, which may be due to the enhanced electron–phonon interactions. It is well known that the thermal expansion of the lattice reduces the interaction between the valence orbitals Br 4p and Pb 6s, thus increasing the bandgap.[54]

To obtain more in-depth information on the charge recombination processes of the 5% Li-doped $CsPbBr_3$ films, the photoluminescence of the films was studied under varying excitation power densities from 50 to 350 mW cm^{-2} using a 450 nm laser. The PL spectra are shown in Fig. 5a for $CsPbBr_3$ and Fig. 5b for 5% Li–$CsPbBr_3$. The results illustrate an increase in the PL intensity with lower excitation power density for the two samples. In addition, the PL intensities of doped film are two times stronger than the pristine ones, which sustain our results on a decrease of defects, and surface passivation.

Under non-resonant excitation conditions, the PL intensity in direct-bandgap semiconductors has a power-law dependence on the excitation density ($I_{Ex.}$), according to the equation below:[57]

$$I_{PL} = I_{Ex.}e^{\beta} \quad (3)$$

with $\beta = 2$ for band-to-band transitions due to exciton or free carrier recombination, $1 < \beta < 2$ for exciton recombination, which includes free excitons and bound excitons, and $\beta < 1$ for free-to-bound recombination and donor–acceptor pairs.[52]

As shown in Fig. 5c, the peak shift has a dependence on the excitation power density, which implies the excitonic nature of the emission. This linear tendency diverges slowly for the Li–$CsPbBr_3$ films. The power-law exponent β was found to be 1.6 ± 0.04 and 1 ± 0.1 for the undoped and 5% Li–$CsPbBr_3$ films. This means that the $CsPbBr_3$ films are governed by exciton recombination, while for the doped $CsPbBr_3$, there is interference between bound pair excitons, free excitons, free-to-bound recombination, and donor–acceptor pair. There is no abrupt increase in the integrated PL intensity below 175 mW cm^{-2} with

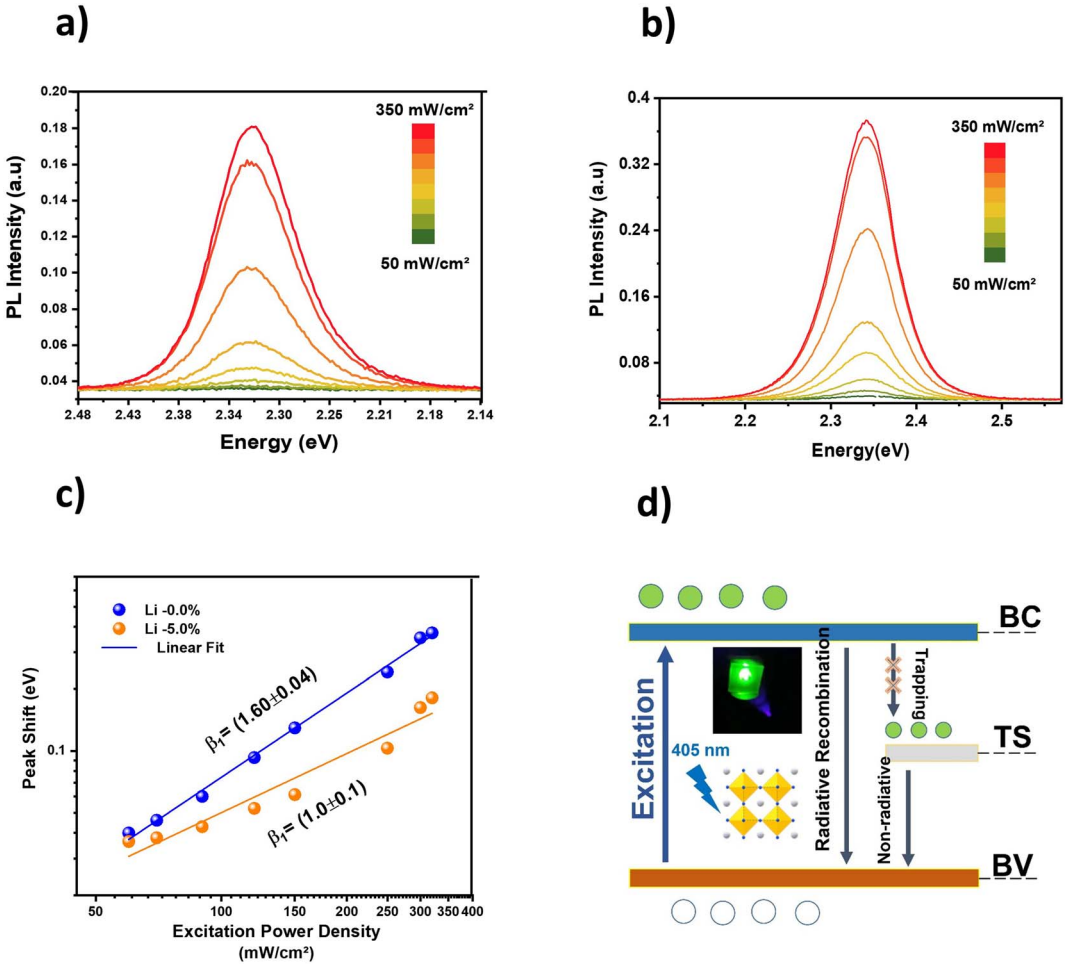

Fig. 5 Power-dependent PL spectra excitation intensity in the range of 50–350 mW cm^{-2} for (a) $CsPbBr_3$; and (b) 5% Li–$CsPbBr_3$. (c) Double-logarithmic PL plots for $CsPbBr_3$ and 5% Li–$CsPbBr_3$ as a function of excitation power density. (d) Schematic illustrating the reduction of the non-radiative recombination process after Li-doping of $CsPbBr_3$ films.

Table 3 Deep defect trap states *vs.* Li doping in $CsPbBr_3$ thin films

Doping of Li (%)	Calculated trap density N_{c_t} (cm^{-3})
0	5.0×10^{17}
2.5	1.5×10^{17}
5	6.0×10^{16}

excitation power density because of spontaneous radiation instead of amplified spontaneous emission or other optical non-linear phenomena.[58]

The decrease of β from 1.6 to 1.0 indicates a decay in non-radiative recombination, as doping induces trap states filled by free electrons. A similar effect has been observed in the doping of $MAPbI_3$ films by Li, as reported by Fang *et al.*[20]

For better illustration of this effect, Fig. 5d shows a schematic of the radiative and non-radiative processes in 5% Li–$CsPbBr_3$, specifically, the reduction of the non-radiative recombination process after the incorporation of Li in the $CsPbBr_3$ films. On the other hand, radiative recombination for the undoped $CsPbBr_3$ films occurs for the electrons located in the conduction band (CB) after having been excited with energies higher than the bandgap. Two recombination processes occur, the first when the electrons return directly to the valence band (VB), and the second when the electrons are trapped in the defect band (DB) located near the bandgap, and subsequently follow a non-radiative path when returning to the VB. For the doped films, the presence of Li in $CsPbBr_3$ film prevents the trapping of electrons by inducing a new energy level (TS), which is more favorable to the radiative recombination path, and thus leads to an increase in the PL emission.

It is clearly seen from the photoluminescence investigations that doping with lithium reduces non-radiative recombination by filling trap states as well as reducing band tail/activation energy. Considering the amount of defect states filled by Li-doping, the trap density was calculated using the equations below, and the obtained values are summarized in Table 3.

$$\text{Reduction in trap state} = \log_{10}(N_t) - (\text{Li}\% \times \log_{10}(N_t)) \quad (4)$$

$$\text{Calculated trap density } (cm^{-3})\ N_{c\_t} = \text{antilog}_{10}(\text{reduction in trap state}) \quad (5)$$

where, N_t is the trap density of $CsPbBr_3$ and N_{c_t} is the calculated trap state after Li doping.

The results show fewer trap states after doping with Li, which may be due to fewer grain boundaries. The same behavior has been observed for doping with other alkali metals in perovskite solar cells, and was attributed to the same factor.[21]

Concluding remarks

In conclusion, lithium doping significantly enhances the structural and photophysical properties of $CsPbBr_3$ perovskite films. The doping improves crystallinity and reduces non-radiative recombination, leading to stronger photoluminescence intensity, particularly at lower temperatures. The surface passivation effect from the alkali cation doping, along with the weakening of electron–phonon coupling, contribute to these positive effects. These findings provide valuable insights into the non-radiative recombination mechanisms, which are crucial for improving the efficiency of perovskite solar cells and the performance of optoelectronic devices. The study suggests that Li-doped $CsPbBr_3$ films hold promise for the development of high-stability, high-performance perovskite thin-film solar cells and optoelectronic devices.

Conflicts of interest

There are no conflicts to declare.

Acknowledgements

The authors would like to thank the LEAP RE initiative, founded by the Ministry of Higher Education, Scientific Research, and Innovation (MESRSI) for the financial support through the project "Environmentally friendly colloidal quantum dots for high performance solar cells"/(QDSOC). M. Bernabé and U. Shaffi would like to thank the Generalitat Valenciana for funding through program PROMETEUS Ref: CIPROM/2022/03.

References

1 P. Teng, X. Han, J. Li, Y. Xu, L. Kang, Y. Wang, Y. Yang and T. Yu, Elegant Face-Down Liquid-Space-Restricted Deposition of $CsPbBr_3$ Films for Efficient Carbon-Based All-Inorganic Planar Perovskite Solar Cells, *ACS Appl. Mater. Interfaces*, 2018, **10**(11), 9541–9546, DOI: 10.1021/acsami.8b00358.

2 X. Liu, X. Tan, Z. Liu, H. Ye, B. Sun, T. Shi, Z. Tang and G. Liao, Boosting the Efficiency of Carbon-Based Planar $CsPbBr_3$ Perovskite Solar Cells by a Modified Multistep Spin-Coating Technique and Interface Engineering, *Nano Energy*, 2019, **56**, 184–195, DOI: 10.1016/j.nanoen.2018.11.053.

3 L. Atourki, M. Bernabé, M. Makha, K. Bouabid, M. Regragui, A. Ihlal, M. Abd-lefdil and M. Mollar, Effect of doping on the phase stability and photophysical properties of CsPbI2Br perovskite thin films, *RSC Adv.*, 2021, **11**, 1440–1449, DOI: 10.1039/D0RA08912E.

4 Y. Jiaoxian, L. Guangxia, C. Chengmin, L. Yan, X. Meirong, W. Tailin, Z. Gang and Z. Lei, Perovskite $CsPbBr_3$ Crystal: Growth and Applications, *J. Mater. Chem. C*, 2020, **8**, 6326–6341, DOI: 10.1039/X0xx00000x.

5 S. Sanchez, N. Christoph, B. Grobety, N. Phung, U. Steiner, M. Saliba and A. Abate, Efficient and Stable Inorganic Perovskite Solar Cells Manufactured by Pulsed Flash Infrared Annealing, *Adv. Energy Mater.*, 2018, **8**(30), 1802060, DOI: 10.1002/aenm.201802060.

6 F. Zhang, C. Xiao, Y. Li, X. Zhang, J. Tang, S. Chang, Q. Pei and H. Zhong, Gram-Scale Synthesis of Blue-Emitting CH3NH3PbBr3 Quantum Dots Through Phase Transfer

Strategy, *Front. Chem.*, 2018, **6**, 444, DOI: 10.3389/fchem.2018.00444.

7 P. G. Papagiorgis, A. Manoli, A. Alexiou, P. Karacosta, X. Karagiorgis, G. Papaparaskeva, C. Bernasconi, M. I. Bodnarchuk, M. V. Kovalenko, T. Krasia-Christoforou and G. Itskos, Robust Hydrophobic and Hydrophilic Polymer Fibers Sensitized by Inorganic and Hybrid Lead Halide Perovskite Nanocrystal Emitters, *Front. Chem.*, 2019, **7**, 87, DOI: 10.3389/fchem.2019.00087.

8 S. S.-Y. Juang, P.-Y. Lin, Y.-C. Lin, Y.-S. Chen, P.-S. Shen, Y.-L. Guo, Y.-C. Wu and P. Chen, Energy Harvesting Under Dim-Light Condition With Dye-Sensitized and Perovskite Solar Cells, *Front. Chem.*, 2019, **7**, 209, DOI: 10.3389/fchem.2019.00209.

9 L. Atourki, M. Bernabé, M. Makha, K. Bouabid, M. Regragui, A. Ihlal, M. Abd-lefdil and M. Mollar, Effect of Doping on the Phase Stability and Photophysical Properties of $CsPbI_2$ Br Perovskite Thin Films, *RSC Adv.*, 2021, **11**(3), 1440–1449, DOI: 10.1039/D0RA08912E.

10 Y. Gao, Y. Wu, Y. Liu, C. Chen, X. Bai, L. Yang, Z. Shi, W. W. Yu, Q. Dai and Y. Zhang, Dual Functions of Crystallization Control and Defect Passivation Enabled by an Ionic Compensation Strategy for Stable and High-Efficient Perovskite Solar Cells, *ACS Appl. Mater. Interfaces*, 2020, **12**(3), 3631–3641, DOI: 10.1021/acsami.9b19538.

11 X. Chang, W. Li, L. Zhu, H. Liu, H. Geng, S. Xiang, J. Liu and H. Chen, Carbon-Based $CsPbBr_3$ Perovskite Solar Cells: All-Ambient Processes and High Thermal Stability, *ACS Appl. Mater. Interfaces*, 2016, **8**(49), 33649–33655, DOI: 10.1021/acsami.6b11393.

12 W. Zhai, J. Lin, C. Li, S. Hu, Y. Huang, C. Yu, Z. Wen, Z. Liu, Y. Fang and C. Tang, Solvothermal Synthesis of Cesium Lead Halide Perovskite Nanowires with Ultra-High Aspect Ratios for High-Performance Photodetectors, *Nanoscale*, 2018, **10**(45), 21451–21458, DOI: 10.1039/C8NR05683H.

13 Y. H. Khattak, F. Baig, A. Shuja, L. Atourki, K. Riaz and B. M. Soucase, Device Optimization of PIN Structured Perovskite Solar Cells: Impact of Design Variants, *ACS Appl. Electron. Mater.*, 2021, 3509–3520, DOI: 10.1021/acsaelm.1c00460.

14 Y. Zhang, W. Zhang, Y. Ye, K. Li, X. Gong and C. Liu, $CsPbBr_3$ Nanocrystal-Embedded Glasses for Luminescent Solar Concentrators, *Sol. Energy Mater. Sol. Cells*, 2022, **238**, 111619, DOI: 10.1016/j.solmat.2022.111619.

15 J. Kang and L.-W. Wang, High Defect Tolerance in Lead Halide Perovskite $CsPbBr_3$, *J. Phys. Chem. Lett.*, 2017, **8**(2), 489–493, DOI: 10.1021/acs.jpclett.6b02800.

16 M. Saliba, T. Matsui, K. Domanski, J.-Y. Seo, A. Ummadisingu, S. M. Zakeeruddin, J.-P. Correa-Baena, W. R. Tress, A. Abate, A. Hagfeldt and M. Grätzel, Incorporation of Rubidium Cations into Perovskite Solar Cells Improves Photovoltaic Performance, *Science*, 2016, **354**(6309), 206–209, DOI: 10.1126/science.aah5557.

17 C. Momblona, L. Gil-Escrig, E. Bandiello, E. M. Hutter, M. Sessolo, K. Lederer, J. Blochwitz-Nimoth and H. J. Bolink, Efficient Vacuum Deposited P-i-n and n-i-p Perovskite Solar Cells Employing Doped Charge Transport Layers, *Energy Environ. Sci.*, 2016, **9**(11), 3456–3463, DOI: 10.1039/C6EE02100J.

18 S. D. Stranks, Nonradiative Losses in Metal Halide Perovskites, *ACS Energy Lett.*, 2017, **2**(7), 1515–1525, DOI: 10.1021/acsenergylett.7b00239.

19 H. Tan, A. Jain, O. Voznyy, X. Lan, F. P. García De Arquer, J. Z. Fan, R. Quintero-Bermudez, M. Yuan, B. Zhang, Y. Zhao, F. Fan, P. Li, L. N. Quan, Y. Zhao, Z.-H. Lu, Z. Yang, S. Hoogland and E. H. Sargent, Efficient and Stable Solution-Processed Planar Perovskite Solar Cells *via* Contact Passivation, *Science*, 2017, **355**(6326), 722–726, DOI: 10.1126/science.aai9081.

20 Z. Fang, H. He, L. Gan, J. Li and Z. Ye, Understanding the Role of Lithium Doping in Reducing Nonradiative Loss in Lead Halide Perovskites, *Adv. Sci.*, 2018, **5**(12), 1800736, DOI: 10.1002/advs.201800736.

21 W. Zhao, Z. Yao, F. Yu, D. Yang and S. F. Liu, Alkali Metal Doping for Improved CH_3 NH_3 PbI_3 Perovskite Solar Cells, *Adv. Sci.*, 2018, **5**(2), 1700131, DOI: 10.1002/advs.201700131.

22 M. Abdi-Jalebi, Z. Andaji-Garmaroudi, S. Cacovich, C. Stavrakas, B. Philippe, J. M. Richter, M. Alsari, E. P. Booker, E. M. Hutter, A. J. Pearson, S. Lilliu, T. J. Savenije, H. Rensmo, G. Divitini, C. Ducati, R. H. Friend and S. D. Stranks, Maximizing and Stabilizing Luminescence from Halide Perovskites with Potassium Passivation, *Nature*, 2018, **555**(7697), 497–501, DOI: 10.1038/nature25989.

23 J. Cao, S. X. Tao, P. A. Bobbert, C. Wong and N. Zhao, Interstitial Occupancy by Extrinsic Alkali Cations in Perovskites and Its Impact on Ion Migration, *Adv. Mater.*, 2018, **30**(26), 1707350, DOI: 10.1002/adma.201707350.

24 J. A. Dawson, A. J. Naylor, C. Eames, M. Roberts, W. Zhang, H. J. Snaith, P. G. Bruce and M. S. Islam, Mechanisms of Lithium Intercalation and Conversion Processes in Organic–Inorganic Halide Perovskites, *ACS Energy Lett.*, 2017, **2**(8), 1818–1824, DOI: 10.1021/acsenergylett.7b00437.

25 Q. Jiang, M. Chen, J. Li, M. Wang, X. Zeng, T. Besara, J. Lu, Y. Xin, X. Shan, B. Pan, C. Wang, S. Lin, T. Siegrist, Q. Xiao and Z. Yu, Electrochemical Doping of Halide Perovskites with Ion Intercalation, *ACS Nano*, 2017, **11**(1), 1073–1079, DOI: 10.1021/acsnano.6b08004.

26 M. Abdi-Jalebi, Z. Andaji-Garmaroudi, A. J. Pearson, G. Divitini, S. Cacovich, B. Philippe, H. Rensmo, C. Ducati, R. H. Friend and S. D. Stranks, Potassium- and Rubidium-Passivated Alloyed Perovskite Films: Optoelectronic Properties and Moisture Stability, *ACS Energy Lett.*, 2018, **3**(11), 2671–2678, DOI: 10.1021/acsenergylett.8b01504.

27 F. Zhang and K. Zhu, Additive Engineering for Efficient and Stable Perovskite Solar Cells, *Adv. Energy Mater.*, 2020, **10**(13), 1902579, DOI: 10.1002/aenm.201902579.

28 L. Kuai, Y. Wang, Z. Zhang, Y. Yang, Y. Qin, T. Wu, Y. Li, Y. Li, T. Song, X. Gao, L. Wang and B. Sun, Passivating Crystal Boundaries with Potassium-Rich Phase in Organic Halide Perovskite, *Sol. RRL*, 2019, **3**(5), 1900053, DOI: 10.1002/solr.201900053.

29 Y. Shi, J. Xi, T. Lei, F. Yuan, J. Dai, C. Ran, H. Dong, B. Jiao, X. Hou and Z. Wu, Rubidium Doping for Enhanced

Performance of Highly Efficient Formamidinium-Based Perovskite Light Emitting Diodes, *ACS Appl. Mater. Interfaces*, 2018, **10**(11), 9849–9857, DOI: 10.1021/acsami.8b00079.

30 J. Jeong, M. Kim, J. Seo, H. Lu, P. Ahlawat, A. Mishra, Y. Yang, M. A. Hope, F. T. Eickemeyer, M. Kim, Y. J. Yoon, I. W. Choi, B. P. Darwich, S. J. Choi, Y. Jo, J. H. Lee, B. Walker, S. M. Zakeeruddin, L. Emsley, U. Rothlisberger, A. Hagfeldt, D. S. Kim, M. Grätzel and J. Y. Kim, Pseudo-Halide Anion Engineering for α-FAPbI3 Perovskite Solar Cells, *Nature*, 2021, **592**(7854), 381–385, DOI: 10.1038/s41586-021-03406-5.

31 S. Ullah, J. Wang, P. Yang, L. Liu, S.-E. Yang, T. Xia, H. Guo and Y. Chen, All-Inorganic $CsPbBr_3$ Perovskite: A Promising Choice for Photovoltaics, *Mater. Adv.*, 2021, **2**(2), 646–683, DOI: 10.1039/D0MA00866D.

32 S. Aharon and L. Etgar, Two Dimensional Organometal Halide Perovskite Nanorods with Tunable Optical Properties, *Nano Lett.*, 2016, **16**(5), 3230–3235, DOI: 10.1021/acs.nanolett.6b00665.

33 Y. Bekenstein, B. A. Koscher, S. W. Eaton, P. Yang and A. P. Alivisatos, Highly Luminescent Colloidal Nanoplates of Perovskite Cesium Lead Halide and Their Oriented Assemblies, *J. Am. Chem. Soc.*, 2015, **137**(51), 16008–16011, DOI: 10.1021/jacs.5b11199.

34 N. Kumar, J. Rani and R. Kurchania, Advancement in $CsPbBr_3$ Inorganic Perovskite Solar Cells: Fabrication, Efficiency and Stability, *Sol. Energy*, 2021, **221**, 197–205, DOI: 10.1016/j.solener.2021.04.042.

35 J. Duan, Y. Zhao, B. He and Q. Tang, Simplified Perovskite Solar Cell with 4.1% Efficiency Employing Inorganic $CsPbBr_3$ as Light Absorber, *Small*, 2018, **14**(20), 1704443, DOI: 10.1002/smll.201704443.

36 J. Liang, C. Wang, Y. Wang, Z. Xu, Z. Lu, Y. Ma, H. Zhu, Y. Hu, C. Xiao, X. Yi, G. Zhu, H. Lv, L. Ma, T. Chen, Z. Tie, Z. Jin and J. Liu, All-Inorganic Perovskite Solar Cells, *J. Am. Chem. Soc.*, 2016, **138**(49), 15829–15832, DOI: 10.1021/jacs.6b10227.

37 Y. Pei, H. Guo, Z. Hu, J. Zhang and Y. Zhu, BiBr3 as an Additive in $CsPbBr_3$ for Carbon-Based All-Inorganic Perovskite Solar Cell, *J. Alloys Compd.*, 2020, **835**, 155283, DOI: 10.1016/j.jallcom.2020.155283.

38 G. Wang, W. Dong, A. Gurung, K. Chen, F. Wu, Q. He, R. Pathak and Q. Qiao, Improving Photovoltaic Performance of Carbon-Based $CsPbBr_3$ Perovskite Solar Cells by Interfacial Engineering Using P3HT Interlayer, *J. Power Sources*, 2019, **432**, 48–54, DOI: 10.1016/j.jpowsour.2019.05.075.

39 H. Wu, J. Qiu, J. Wang, Y. Wen, Q. Wang, Z. Long, D. Zhou, Y. Yang and D. Wang, The Dual-Defect Passivation Role of Lithium Bromide Doping in Reducing the Nonradiative Loss in $CsPbX_3$ (X = Br and I) Quantum Dots, *Inorg. Chem. Front.*, 2021, **8**(3), 658–668, DOI: 10.1039/D0QI01262A.

40 D. Wang, J. Qiu, D. Zhou, S. Hu, Y. Wen, K. Zhang, Q. Wang, Y. Yang, H. Wu, Z. Long, X. Li, J. Pi and E. Cao, Lithium Doping Induced Self-Crystallization of $CsPbBr_3$ Nanocrystal Glass with Improved Quantum Yield and Stability, *Chem. Eng. J.*, 2021, **421**, 127777, DOI: 10.1016/j.cej.2020.127777.

41 A. Subramanian, Z. Pan, Z. Zhang, I. Ahmad, J. Chen, M. Liu, S. Cheng, Y. Xu, J. Wu, W. Lei, Q. Khan and Y. Zhang, Interfacial Energy-Level Alignment for High-Performance All-Inorganic Perovskite $CsPbBr_3$ Quantum Dot-Based Inverted Light-Emitting Diodes, *ACS Appl. Mater. Interfaces*, 2018, **10**(15), 13236–13243, DOI: 10.1021/acsami.8b01684.

42 M. C. Brennan, M. Kuno and S. Rouvimov, Crystal Structure of Individual $CsPbBr_3$ Perovskite Nanocubes, *Inorg. Chem.*, 2019, **58**(2), 1555–1560, DOI: 10.1021/acs.inorgchem.8b03078.

43 Z. Tang, S. Uchida, T. Bessho, T. Kinoshita, H. Wang, F. Awai, R. Jono, M. M. Maitani, J. Nakazaki, T. Kubo and H. Segawa, Modulations of Various Alkali Metal Cations on Organometal Halide Perovskites and Their Influence on Photovoltaic Performance, *Nano Energy*, 2018, **45**, 184–192, DOI: 10.1016/j.nanoen.2017.12.047.

44 M. Ouafi, L. Atourki, L. Laânab, E. Vega, B. Mari, M. Mollar and B. Jaber, Hot Airflow Deposition: Toward High Quality MAPbI3 Perovskite Films, *J. Alloys Compd.*, 2019, **790**, 1101–1107, DOI: 10.1016/j.jallcom.2019.03.187.

45 M. Kulbak, D. Cahen and G. Hodes, How Important Is the Organic Part of Lead Halide Perovskite Photovoltaic Cells? Efficient $CsPbBr_3$ Cells, *J. Phys. Chem. Lett.*, 2015, **6**(13), 2452–2456, DOI: 10.1021/acs.jpclett.5b00968.

46 A. Dey, P. Rathod and D. Kabra, Role of Localized States in Photoluminescence Dynamics of High Optical Gain $CsPbBr_3$ Nanocrystals, *Adv. Opt. Mater.*, 2018, **6**(11), 1800109, DOI: 10.1002/adom.201800109.

47 H. Min, M. Kim, S.-U. Lee, H. Kim, G. Kim, K. Choi, J. H. Lee and S. I. Seok, Efficient, Stable Solar Cells by Using Inherent Bandgap of a-Phase Formamidinium Lead Iodide, *Science*, 2019, **366**, 749–753.

48 X. B. Zhang, T. Taliercio, S. Kolliakos and P. Lefebvre, Influence of Electron-Phonon Interaction on the Optical Properties of III Nitride Semiconductors, *J. Phys.: Condens. Matter*, 2001, **13**(32), 7053–7074, DOI: 10.1088/0953-8984/13/32/312.

49 B. Ai, C. Liu, Z. Deng, J. Wang, J. Han and X. Zhaoa, Low Temperature Photoluminescence Properties of $CsPbBr_3$ Quantum Dots Embedded in Glasses, *Phys. Chem. Chem. Phys.*, 2016, **18**(1), 21–46, DOI: 10.1039/C5CP05142H.

50 A. Shinde, R. Gahlaut and S. Mahamuni, Low-Temperature Photoluminescence Studies of $CsPbBr_3$ Quantum Dots, *J. Phys. Chem. C*, 2017, **121**(27), 14872–14878, DOI: 10.1021/acs.jpcc.7b02982.

51 M. Leroux, N. Grandjean, B. Beaumont, G. Nataf, F. Semond, J. Massies and P. Gibart, Temperature Quenching of Photoluminescence Intensities in Undoped and Doped GaN, *J. Appl. Phys.*, 1999, **86**(7), 3721–3728, DOI: 10.1063/1.371242.

52 H. He, Q. Yu, H. Li, J. Li, J. Si, Y. Jin, N. Wang, J. Wang, J. He, X. Wang, Y. Zhang and Z. Ye, Exciton Localization in Solution-Processed Organolead Trihalide Perovskites, *Nat. Commun.*, 2016, **7**(1), 10896, DOI: 10.1038/ncomms10896.

53 H. Cho, C. Wolf, J. S. Kim, H. J. Yun, J. S. Bae, H. Kim, J. Heo, S. Ahn and T. Lee, High-Efficiency Solution-Processed Inorganic Metal Halide Perovskite Light-Emitting Diodes, *Adv. Mater.*, 2017, **29**(31), 1700579, DOI: **10.1002/adma.201700579**.

54 A. Shinde, R. Gahlaut and S. Mahamuni, Low-Temperature Photoluminescence Studies of $CsPbBr_3$ Quantum Dots, *J. Phys. Chem. C*, 2017, **121**(27), 14872–14878, DOI: **10.1021/acs.jpcc.7b02982**.

55 K. Wu, A. Bera, C. Ma, Y. Du, Y. Yang, L. Li and T. Wu, Temperature-Dependent Excitonic Photoluminescence of Hybrid Organometal Halide Perovskite Films, *Phys. Chem. Chem. Phys.*, 2014, **16**(41), 22476–22481, DOI: **10.1039/C4CP03573A**.

56 Z. Liu, Q. Shang, C. Li, L. Zhao, Y. Gao, Q. Li, J. Chen, S. Zhang, X. Liu, Y. Fu and Q. Zhang, Temperature-Dependent Photoluminescence and Lasing Properties of $CsPbBr_3$ Nanowires, *Appl. Phys. Lett.*, 2019, **114**(10), 101902, DOI: **10.1063/1.5082759**.

57 M. Sebastian, J. A. Peters, C. C. Stoumpos, J. Im, S. S. Kostina, Z. Liu, M. G. Kanatzidis, A. J. Freeman and B. W. Wessels, Excitonic Emissions and Above-Band-Gap Luminescence in the Single-Crystal Perovskite Semiconductors CsPbB r 3 and CsPbC l 3, *Phys. Rev. B*, 2015, **92**(23), 235210, DOI: **10.1103/PhysRevB.92.235210**.

58 Y. Wang, M. Zhi, Y.-Q. Chang, J.-P. Zhang and Y. Chan, Stable, Ultralow Threshold Amplified Spontaneous Emission from $CsPbBr_3$ Nanoparticles Exhibiting Trion Gain, *Nano Lett.*, 2018, **18**(8), 4976–4984, DOI: **10.1021/acs.nanolett.8b01817**.